Ultrasensitivity of the *Bacillus subtilis* sporulation decision

Jatin Narula[a], Seram N. Devi[b], Masaya Fujita[b,1], and Oleg A. Igoshin[a,1]

[a]Department of Bioengineering, Rice University, Houston, TX 77030; and [b]Department of Biology and Biochemistry, University of Houston, Houston, TX 77204-5001

Edited by Richard Losick, Harvard University, Cambridge, MA, and approved October 24, 2012 (received for review August 14, 2012)

Starving *Bacillus subtilis* cells execute a gene expression program resulting in the formation of stress-resistant spores. Sporulation master regulator, Spo0A, is activated by a phosphorelay and controls the expression of a multitude of genes, including the forespore-specific sigma factor σ^F and the mother cell-specific sigma factor σ^E. Identification of the system-level mechanism of the sporulation decision is hindered by a lack of direct control over Spo0A activity. This limitation can be overcome by using a synthetic system in which Spo0A activation is controlled by inducing expression of phosphorelay kinase KinA. This induction results in a switch-like increase in the number of sporulating cells at a threshold of KinA. Using a combination of mathematical modeling and single-cell microscopy, we investigate the origin and physiological significance of this ultrasensitive threshold. The results indicate that the phosphorelay is unable to achieve a sufficiently fast and ultrasensitive response via its positive feedback architecture, suggesting that the sporulation decision is made downstream. In contrast, activation of σ^F in the forespore and of σ^E in the mother cell compartments occurs via a cascade of coherent feed-forward loops, and thereby can produce fast and ultrasensitive responses as a result of KinA induction. Unlike σ^F activation, σ^E activation in the mother cell compartment only occurs above the KinA threshold, resulting in completion of sporulation. Thus, ultrasensitive σ^E activation explains the KinA threshold for sporulation induction. We therefore infer that under uncertain conditions, cells initiate sporulation but postpone making the sporulation decision to average stochastic fluctuations and to achieve a robust population response.

cell fate | development | differentiation | stochasticity | network

In response to nutrient deprivation, *Bacillus subtilis* cells undergo asymmetrical cell division and then follow a cell differentiation program resulting in formation of metabolically inert spores (1, 2) (Fig. 1*A*). Sporulation requires the execution of a complex gene expression program involving hundreds of "sporulation" genes (3–6). The availability of a large number of genetic mutants that differ from the WT only in their sporulation response makes *B. subtilis* an ideal model system to study the relationship between gene expression and cell fate specification during bacterial differentiation (7).

Progression of the sporulation program is under the control of a large regulatory network (hereafter called the sporulation network). This network involves the sporulation master regulator Spo0A and five alternative sigma factors (σ^H, σ^F, σ^E, σ^K, and σ^G) that are activated in precise temporal order (8). Initiation of the sporulation program is controlled by Spo0A (4, 9). The activity and concentration of this master transcription factor are regulated by phosphorelay through both posttranslational and transcriptional interactions (10). Posttranslationally, phosphoryl groups are transferred from one of the five autophosphorylating kinases (KinA–KinE) to Spo0A via the phosphotransferases Spo0B and Spo0F (Fig. 1*B*). Moreover, phosphorylated Spo0F and Spo0A are subject to negative regulation by the phosphatases RapA and Spo0E, respectively (11). Transcriptionally, expression of genes for KinA, Spo0F, and Spo0A are regulated by the activated form of Spo0A (phosphorylated form of Spo0A, hereafter called Spo0A~P) directly and indirectly via multiple feedback loops (Fig. 1*B*).

As Spo0A~P accumulates, it activates the expression of sporulation genes and promotes polar septation, resulting in the formation of a small forespore compartment and a larger mother cell compartment inside the cell (12) (Fig. 1*A*). Subsequently, compartment-specific sigma factors σ^F and σ^E are activated in the forespore and the mother cell, respectively (8) (Fig. 1*C*). The σ^F-bound and σ^E-bound RNA polymerases (RNAPs) direct the compartment-specific gene expression programs, including the activation of the late-stage sigma factors σ^G and σ^K. Morphological changes resulting in the production of a mature spore are directed by each of these sigma factors in a temporally and spatially controlled manner (5, 6).

Although the molecular interactions in the sporulation network have been mapped out, it is not clear how this network processes environmental and metabolic signals to achieve distinct cell fate decisions. Moreover, even in an isogenic population of starving cells, only a fraction of them form spores (13). This variability in cell fate is likely to be part of a bet-hedging strategy to manage the risks and benefits of the sporulation decision (13, 14), but the implementation mechanism for this strategy is unknown. In particular, it is not clear activation of which sporulation network component signifies the sporulation decision and thereby serves as a reliable predictor of cell fate.

Several previous studies have hypothesized that sporulation is triggered in cells reaching a threshold level of Spo0A~P (14–18). This hypothesis is motivated by the observation that an increase in Spo0A~P is sufficient to shift the site of cell division to an asymmetrical polar site, and thereby to initiate sporulation (19, 20). However, the hypothesis of a single Spo0A~P threshold has been undermined by recent studies showing that (*i*) starving populations of *B. subtilis* exhibit broad and unimodal distributions of Spo0A activity (16, 17, 21) and (*ii*) there is significant overlap in distributions of Spo0A activity in sporulating and nonsporulating cells (22). Moreover, cells that form an asymmetrical septum but do not activate σ^F and/or σ^E are able to resume vegetative growth (23–25). These results suggest that the process of sporulation only becomes irreversible upon σ^F and σ^E activation in the forespore and mother cell, respectively. Therefore, to understand the sporulation decision on a system level, we must establish how Spo0A~P levels control σ^F and σ^E activation.

To uncover the relationship between Spo0A~P levels and the activities of the downstream sigma factors, we need a way to

Author contributions: J.N., M.F., and O.A.I. designed research; J.N., S.N.D., M.F., and O.A.I. performed research; J.N., S.N.D., and M.F. analyzed data; and J.N., M.F., and O.A.I. wrote the paper.

The authors declare no conflict of interest.

This article is a PNAS Direct Submission.

[1]To whom correspondence may be addressed. E-mail: mfujita@uh.edu or igoshin@rice.edu.

See Author Summary on page 20196 (volume 109, number 50).

This article contains supporting information online at www.pnas.org/lookup/suppl/doi:10.1073/pnas.1213974109/-/DCSupplemental.

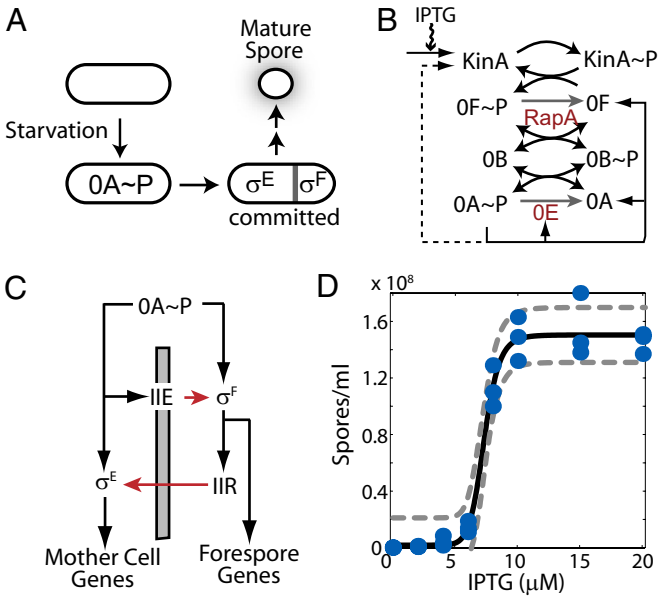

Fig. 1. Regulation of sporulation in *B. subtilis*. (*A*) Starvation triggers a switch from vegetative growth to sporulation and activates the sporulation master regulator Spo0A~P (0A~P). 0A~P promotes the formation of asymmetrical septa and activates sigma factors σ^F and σ^E in the forespore and the mother cell, respectively. Only cells with active σ^F and σ^E are committed to progress through several additional stages before a mature spore appears. (*B*) Sporulation phosphorelay transfers phosphoryl groups from the kinases KinA–E (only KinA is shown) to the master regulator Spo0A via two phosphotransferases, Spo0B (0B) and Spo0F (0F). 0A~P controls the expression of multiple genes in the phosphorelay through transcriptional feedback. KinA expression is indirectly regulated by 0A~P (dashed arrow) in the WT phosphorelay, but in the ASI system, the KinA promoter is replaced with an IPTG-inducible promoter (solid arrow). (*C*) Sporulation network is hierarchically organized. 0A~P directly controls the expression of σ^F and indirectly controls its activation [via SpoIIE (IIE) anchored in the polar septum, gray bar]. 0A~P also controls the expression of σ^E and its activation via the σ^F-regulated expression of SpoIIR (black and red arrows show transcriptional and posttranslational regulatory interactions, respectively). (*D*) At a threshold level of KinA induction, spore counts increase dramatically (~20-fold increase in spore count between 4 μM and 10 μM IPTG) to match WT sporulation levels. The blue circles represent experimentally measured spore counts. The solid and dashed lines represent the Hill equation fit and 95% confidence intervals, respectively.

interrogate the sporulation network systematically with perturbations of Spo0A~P levels. Such perturbations can be controllably achieved by using synthetic biology methods to rewire the naturally occurring networks (26). To apply these methods for phosphorelay, we use a synthetic artificial sporulation initiation (ASI) system, which allows for tunable control of Spo0A~P activity by artificially tuning the KinA level from an isopropyl-β-D-thiogalactopyranoside (IPTG)–inducible promoter (27, 28) (Fig. 1*B*). In this synthetic system, phosphate flux through the phosphorelay that activates Spo0A can be directly regulated by added inducer, and the resulting changes in the activities of downstream sigma factors σ^F and σ^E can be simultaneously monitored using the *lacZ* or fluorescent reporter gene constructs. Recently, this system has been used to show that induction of KinA to a concentration normally achieved in starving WT cells leads to a large number of spores, even in rich media (27) (Fig. 1*D*). Thus, the ASI decouples starvation signaling from downstream events in the sporulation network and allows us to study downstream signal processing networks while minimizing the effects of "extrinsic noise" (i.e., factors resulting from variations in local cell density, cell size, growth rate, and other global parameters). Such factors can significantly influence sporulation of WT cells in starvation conditions (13).

In this study, by combining quantitative experiments using an ASI system with detailed mathematical modeling, we uncover the relationship between the levels of KinA activity, Spo0A~P, and the activities of σ^F and σ^E. Comparing the fractions of cells with each regulator activated with the fraction of sporulating cells at different levels of KinA activity, we determine the point at which the sporulation decision is finalized. Finally, the relevance of the uncovered facts is verified in the WT cells under starvation conditions. Thus, our results provide a system-level picture on how the sporulation network makes appropriate cell fate decisions.

Results

Sporulation in ASI Is Induced in an Ultrasensitive Manner. Previously, we have shown that the ASI system can efficiently induce sporulation in rich medium when KinA is induced to a level that matches KinA concentrations in WT cells in sporulation media (27). Notably, in these experiments, the number of cells forming spores increases sharply in a small range of IPTG concentrations (27). As a result, an increase in IPTG concentration between 4 μM and 10 μM IPTG leads to about a 20-fold increase in the number of spore-forming cells. Such responses are often referred to as ultrasensitive; mathematically, they can be characterized by a large value of slope in log-log coordinates (x is an input and y is an output):

$$\frac{d\log(y)}{d\log(x)} = \frac{dy/y}{dx/x} \gg 1$$

or an equivalently large effective Hill coefficient, n, when the Hill equation $y = b + fx^n/(K^n + x^n)$ is fitted to data.

By repeating these experiments, we verified that spore counts increase ultrasensitively in response to the increasing IPTG concentrations (Fig. 1*D*). If fitted by the Hill equation, the curves can be characterized by the Hill exponent $n \sim 12$ with a 95% confidence interval of 7.5–16.5. The threshold amount of IPTG triggering sporulation is even more robust, with a mean level of $K = 7.3$ μM and a 95% confidence interval of 7.0–7.6 μM. Ultrasensitive increase in spore counts cannot be attributed to the response of IPTG-inducible promoter because the averaged KinA concentration (in cell culture) increases less than twofold between 4 μM and 10 μM IPTG (Fig. S1*A*; effective Hill coefficient of KinA induction is $n \sim 2.0$). Notably, single-cell distributions of KinA concentration measured at 4 μM and 10 μM IPTG are unimodal but noisy and partially overlapping (Fig. S1*B*).

Ultrasensitivity in the population response can be explained if we assume that the level of some downstream gene essential for sporulation increases ultrasensitively as a function of KinA in single cells (Fig. S1). As a result, noisy unimodal distribution of KinA will be converted into a bimodal distribution of the downstream gene and the fraction of cells in each peak will ultrasensitively depend on the mean level of KinA (Fig. S1 *C* and *D*). To confirm this, we used a toy theoretical model that introduces a hypothetical downstream gene that ultrasensitively depends on KinA (a Hill function with $n = 20$; Fig. S1*D*).We tuned the parameters of KinA induction to match the mean level and distribution of KinA observed in the experiments and then calculated the expected population distribution of the hypothetical downstream gene. Resulting fractions of simulated cells in which these downstream genes were activated are in good agreement with the observed fraction of sporulating cells (Fig. S1*E*). Based on this, we hypothesize that the abrupt increase in the number of sporulating cells above the threshold level of KinA originates from ultrasensitivity of the sporulation network in individual cells. In the following sections, we test this hypothesis and uncover the mechanism for generating such an ultrasensitive transfer function.

Activation of Spo0A Is Not Ultrasensitive. To establish how induction of KinA expression affects Spo0A activation, we first built a model for the phosphorelay module. The model includes the transcriptional regulation of module components and their posttranslational modifications by phosphotransfer reactions. The model inputs the concentration of IPTG, which is converted to parameters of KinA transcription to ensure agreement of the model predictions with the observed mean and SD of KinA concentration at all IPTG levels. To maintain consistency with experimental results, we report Spo0A~P levels in terms of transcriptional activity of the high-threshold Spo0A~P target *spoIIG* promoter (*PspoIIG*) (29). Throughout this section, we define Spo0A activity as the *PspoIIG* transcription level by experimentally measuring β-galactosidase activity derived from *PspoIIG-lacZ*, measuring GFP intensity derived from *PspoIIG-gfp*, or computing the transcription rate in the model.

Our model showed that the increase in Spo0A activity as a function of KinA can either be graded (Fig. 2*A*, green curve) or ultrasensitive (Fig. 2*A*, purple curve) depending on the parameter values selected (Fig. 2*A*). The sensitivity of the phosphorelay response to IPTG (IPTG-Spo0A~P transfer function) critically depends on the strength of the transcriptional positive feedbacks from Spo0A~P to Spo0A and Spo0F (Fig. S2*A*). Parameter sets with strong positive feedback, for example, those with a high Hill coefficient for the effect of Spo0A~P on the activation of *Pspo0A* and *Pspo0F* (transcription from the promoters of *spo0A* and *spo0F*, respectively) display ultrasensitivity, whereas weaker feedback leads to graded IPTG-Spo0A~P transfer functions (Fig. S2*A*). Notably, ultrasensitive increases in Spo0A~P as a function of IPTG occur for phosphorelay module parameter values for which the module is a bistable switch (Fig. 2*A*, purple curve, and Fig. S2*A*). Thus, if the decision to sporulate was directly determined by the level of Spo0A~P, a bistable phosphorelay response could explain why the spore count rises so sharply from 4 μM to 10 μM IPTG.

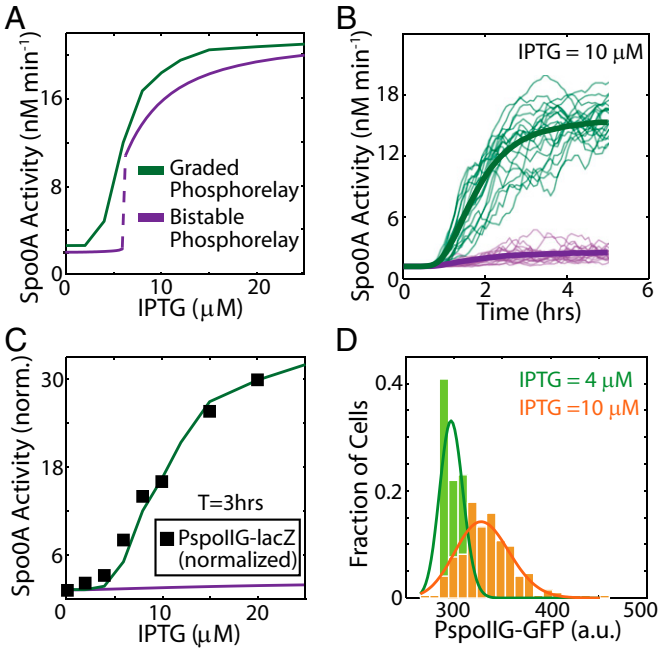

Fig. 2. Phosphorelay response is not ultrasensitive, due to response time requirements. (*A*) Modeling results show that the steady-state Spo0A activity computed as the rate of PspoIIG transcription can either be graded (green curve) or bistable and ultrasensitive (purple curve). (*B*) Stochastic simulations show that at 10 μM IPTG, PspoIIG expression increases significantly by 3 h after induction for the graded (green curves) phosphorelay, whereas bistable (purple curves) phosphorelay shows little change in expression from PspoIIG. Thin curves are individual stochastic simulation trajectories, and thick curves indicate the average of 400 such trajectories. (*C*) Measurements of the increase in Spo0A activity at T3 as a function of IPTG with a PspoIIG-lacZ reporter (■) match the predicted response of the graded phosphorelay (green curve) but not the bistable phosphorelay (purple curve). All values are normalized by the value at 0 μM IPTG. (*D*) In agreement with the graded phosphorelay model, single-cell measurements of GFP expression from the *spoIIG* promoter at T1 show no bimodality at either 4 μM or 10 μM IPTG and can be fit with gamma distributions (solid curves). a.u., arbitrary units.

However, our simulations indicated that the bistable phosphorelay would show negligible increase in Spo0A activity even up to 6 h (T6; hereafter T*n* will denote time of *n* hours after IPTG addition) (Fig. 2*B*, purple curve, and Fig. S2*B*). Because a large number of phase-bright endospores are formed at IPTG = 10 μM by T6 (27), these results (Fig. 2*B*) suggest that in the bistable parameter regime, the phosphorelay response is unrealistically slow. We note here that even the graded phosphorelay does not achieve steady state within 3 h of induction (Fig. 2*B*, green curves). Therefore, we must use the computed dynamical transfer function (rather than the steady-state transfer function) of the phosphorelay to compare the modeling results with experimental data. We have found in our experiments with the ASI system that most cells reach the point of engulfment by 3 h after induction with IPTG. This indicates that most cells have reached a decision about cell fate by T3. Therefore, it is a suitable time point at which to evaluate the output of our models. Focusing on transcriptional activity of *PspoIIG* at T3, we found that the bistable phosphorelay model showed little increase in it even at high IPTG concentrations (Fig. 2*C*, purple curve), whereas the graded phosphorelay model predicted a 30-fold increase over the range of IPTG simulated (Fig. 2*C*, green curve). However, the graded model of the phosphorelay showed only a fivefold change in *PspoIIG* expression between 4 μM and 10 μM (Fig. 2*C*; green curve, average of stochastic simulations; Hill coefficient for fit to experimental data, $n \sim 2.4$), which is insufficient to explain the ultrasensitive response of spore formation (Fig. 1*D*).

Taken together, the modeling results suggest that only the graded phosphorelay model is sufficiently fast to explain the sporulation dynamics. To confirm this prediction, we experimentally analyzed the input–output dynamics of the phosphorelay module. We measured Spo0A activity using a *PspoIIG-lacZ* (output) reporter at different IPTG concentrations (input). As shown in Fig. 2*C* (■), the experimentally measured Spo0A activity closely matched the predictions of the graded phosphorelay model, suggesting that the phosphorelay module response is not bistable, and thus not the determinant of the ultrasensitive increase in spore formation. To test the graded phosphorelay model further, we quantified Spo0A activity in single cells with a *PspoIIG-gfp* reporter to determine whether the distributions show bimodality indicative of a bistable or ultrasensitive phosphorelay response. Although the GFP expression level from *PspoIIG* at T1 was highly heterogeneous, we found that the distributions are not bimodal (Fig. 2*D*). Moreover, the peaks corresponding to low (4 μM) and high (10 μM) IPTG levels are not well separated.

Thus, our results agree with several recent reports that have shown cell fate heterogeneity during sporulation is not associated with bimodality of Spo0A~P activity (16, 17). Altogether, these results lead us to conclude that the phosphorelay response or Spo0A~P concentration does not increase steeply around the KinA threshold and that the ultrasensitivity in the sporulation response must be associated with network components that reside downstream of the phosphorelay.

Activation of σ^F in the Forespore Is Ultrasensitive but Occurs Below the Sporulation Threshold. To test whether the σ^F module is the determinant of the ultrasensitive cell fate decision, we first modeled this module separately to compute its input–output properties

and then integrated it with the phosphorelay module to establish its response to KinA induction.

The σ^F activation module has been studied extensively both experimentally and theoretically. These studies have shown that σ^F (SpoIIAC) expression from the *spoIIA* operon is turned on at a relatively low concentration of Spo0A~P before septation (8). The anti-sigma factor SpoIIAB and anti–anti-sigma factor SpoIIAA are expressed, along with σ^F from the *spoIIA* operon (30). The SpoIIAB kinase inactivates SpoIIAA and forms a complex with σ^F, preventing it from interacting with RNAP (31) (Fig. S3*A*; details are provided in *SI Materials and Methods*). Compartment-specific activation of σ^F in the forespore is achieved when the polar septum forms, and the subsequent preferential localization of septum-bound phosphatase SpoIIE on the forespore side leads to an effective increase in its concentration in the forespore compartment. As a result, SpoIIE dephosphorylates SpoIIAA, leading to the activation of σ^F in a forespore compartment-specific manner (32). Mathematical models of the σ^F activation network have shown that the activity of σ^F increases ultrasensitively with an increase in SpoIIE concentration (33, 34).

To determine how phosphorelay activity affects σ^F activation, we extended our earlier models to include regulation of *spoIIA* and *spoIIE* gene expression by Spo0A~P. We found that the threshold of SpoIIE concentration, around which σ^F activity increases, is dependent on the expression levels of the *spoIIA* operon (Fig. S3*B*). Moreover, because Spo0A~P controls both *spoIIA* and *spoIIE* transcription, the regulation of the σ^F module can be defined as an AND-type coherent feed-forward (6) (Fig. 1*C*). AND-type coherent feed-forward loops combine the sensitivity of each branch (35), which can potentially lead to ultrasensitive responses (Eq. **S9** in *SI Materials and Methods*). In our case, we note that Spo0A~P regulates both *spoIIA* and *spoIIE* cooperatively [Hill exponents: n_{IIA}, $n_{IIE} > 2$ (36)]. This cooperativity is amplified by the feed-forward loop because σ^F activation itself is highly ultrasensitive as a function of SpoIIE concentration (Fig. S3*B*). Based on these facts, we expect that even the modest increase in the level of Spo0A~P seen in the previous section could result in an ultrasensitive increase in σ^F activity.

The results of our simulations corroborated this rationale, but, surprisingly, the model predicted that σ^F activation would increase ultrasensitively at low IPTG concentrations (Fig. 3*A*). The Hill equation fit for σ^F activity as a function of IPTG concentration (Fig. 3*A*, dashed black curve) indicates a threshold of 4 μM IPTG (95% confidence interval: 3.9–4.2 μM) and a Hill coefficient of $n \sim 4.6$. At the population level, σ^F activity has a bimodal distribution and about half of the cells show significant σ^F activity at 4 μM IPTG when less than 1% of cells actually end up as spores (Fig. 3*D*, purple dots). Moreover, our model predicted that the fraction of cells activating σ^F (we chose 2 μM σ^F as a threshold) increases less than twofold from 50% to 77% between 4 μM and 10 μM IPTG (Fig. 3*D*, black curve). This is in stark contrast to the experimentally observed increase in the fraction of spores (Fig. 3*D*, blue dots), which increases 20-fold between 4 μM and 10 μM IPTG.

These results indicate that the threshold of KinA for σ^F activation falls below the observed value for the sporulation response because transcription of both *spoIIA* and *spoIIE* occurs at a relatively low Spo0A~P threshold (37). As a result, both operons are expressed at high levels even at low IPTG concentrations (4 μM IPTG) for KinA induction. Inevitably then, under such conditions, cells accumulate sufficient SpoIIE to activate σ^F after septation. Our prediction that a large fraction of cells activate σ^F even at low IPTG is robust to the choice of threshold concentration for which we consider σ^F to be "activated." This robustness is due to the bimodality of the active σ^F concentration in the population (Fig. 3*B*, *Lower*); the fractions of activated cells would not change much as long as the threshold level is between the peaks.

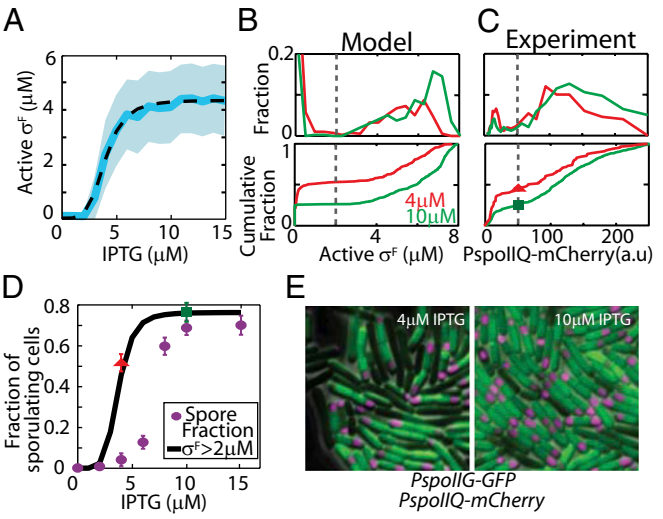

Fig. 3. σ^F activation overestimates the fraction of cells that sporulate. (*A*) Stochastic simulations of a mathematical model integrating phosphorelay and σ^F activation modules show ultrasensitive increases of σ^F in single cells as a function of IPTG (mean response, solid blue line; SD, shaded area; Hill equation fit, dashed black line). However, only a twofold increase in the mean active σ^F level is observed between 4 μM and 10 μM IPTG because σ^F activation has a low threshold (~4 μM IPTG). Bimodal distributions of active σ^F level in the model (*B*, *Upper*) and in single-cell experiments with *PspoIIQ-mCherry* reporter (*C*, *Upper*) are shown. (*B* and *C*) Cumulative distributions (*Lower*) corresponding to the data (*Upper*) are shown (i.e., total fraction of cells with an active σ^F level below the given value). Threshold values separating two peaks (gray bars) are chosen to predict the fraction of cells that activate σ^F in *D*. a.u., arbitrary units. (*D*) Model predictions for fraction of sporulating cells based on the threshold of active σ^F level (black curve) are computed using the distributions for various IPTG levels and the threshold value shown in *B*. Experimental data (red triangle and green square for 4 μM and 10 μM, respectively) are obtained using the threshold and distributions in *C*. Fractions of σ^F-active cells computed from experimental and simulation data are in excellent agreement with one another, but both exceed observed spore fractions (purple dots; calculated from spore counts shown in Fig. 1*D* using Eq. **1** in *Materials and Methods*). (*E*) Examples of the microscopy data of strain MF3765 used to construct distributions in *C*. A significant fraction of cells show σ^F activity (measured by *PspoIIQ-mCherry* false-colored magenta forespore in the image) even at low IPTG concentrations (*Left*, 4 μM). This fraction increases at high IPTG (*Right*, 10 μM), but the increase is not ultrasensitive. Spo0A activity was measured by *PspoIIG-gfp* (green). The images show a field of view of 20 × 20 μm.

Our model also demonstrated that despite the ultrasensitivity of the σ^F activation module, σ^F is activated within ~10 min of septation (Fig. S3*D*). This result is in contrast to the dynamic behavior of the phosphorelay network, where there is a tradeoff between the ultrasensitivity and response time of Spo0A~P activation (Fig. 2 *A*–*C* and Fig. S2 *A* and *B*). This tradeoff is avoided in the σ^F activation module because ultrasensitivity is achieved through coherent feed-forward rather than positive feedback architecture (Fig. 1*C*). Moreover, an increase in *spoIIA* and *spoIIE* transcription does not slow down the response of the σ^F module because the gene products of both accumulate before septation under Spo0A~P control; thus, the rate of σ^F activation is only determined by relatively fast posttranslational reactions in the forespore. In fact, the rapid activation of σ^F is known to be essential for its role in intercompartmental signaling after septation (25, 38).

We confirmed our model predictions for the σ^F module experimentally by tracking Spo0A and σ^F activities simultaneously using *PspoIIG-gfp* and *PspoIIQ-mCherry* as reporters (MF3765; here and below, strain numbers are shown as in Table S1 and primers used in Table S2), respectively (Fig. 3*E*). We found

that the σ^F activity displays a bimodal distribution and only a fraction of cells activate significant levels of σ^F (Fig. 3 *C* and *D* and Fig. S3*E*). In agreement with model predictions, our results indicated a relatively large fraction of σ^F-active cells (55 ± 2.5%, average ± SD of five independent measurements; details are provided in *Materials and Methods*) even at 4 μM IPTG (sub-threshold level of KinA). Accordingly, the increase in the fraction of cells that activate σ^F between 4 μM and 10 μM (σ^F-active cells increase from 55% of cells counted at 4μM to 74.25 ± 2.5% of cells counted at 10 μM) matched our predictions of the response of the σ^F module to KinA induction. As shown in Fig. 3*D*, the red triangle (4 μM) and the green square (10 μM) corresponded to the fraction of cells with σ^F reporter intensity above the threshold selected in Fig. 3*C* and matched the model predictions (black curve) but not the measured spore fractions (purple dots; calculated from spore counts in Fig. 1*D* and viable cell counts; Eq. **1** in *Materials and Methods*). Based on these results, we can rule out σ^F activation as a determinant of cell fate ultrasensitivity around the KinA threshold.

Ultrasensitive σ^E Activation in the Mother Cell Determines Cell Fate. We extended our approach of modular analysis of the sporulation network further downstream to determine if activation of σ^E is the decision point for the ultrasensitive cell fate response. Analogous to previous sections, we first model the σ^E module in isolation and thereafter integrate it with the models of the σ^F activation module and the phosphorelay.

The σ^E module is regulated at several different levels as follows: (*i*) Spo0A~P stimulates transcription of the *spoIIG* operon encoding both pro-σ^E (inactive form of σ^E) and its processing enzyme SpoIIGA preferentially in the mother cell (39), and (*ii*) in the forespore, the gene for the SpoIIGA activation signal, SpoIIR, is transcribed by σ^F-RNAP (thus indirectly controlled by Spo0A~P) (40) (Fig. S4*A*). As a result, the active form of σ^E is produced at a level sufficient to transcribe genes in its regulon only after the completion of polar septation and σ^F activation (5). Therefore, similar to the σ^F module, the σ^E module is controlled both directly and indirectly by Spo0A~P via an AND-type coherent feed-forward loop that can amplify the degree of response sensitivity (8).

The level of activated σ^E depends on the rate of proteolytic cleavage of its propeptide, and hence on the concentrations of both SpoIIGA and SpoIIR as well as the amount of pro-σ^E available for activation. Our model supported the above notion that a combined increase in both SpoIIGA and SpoIIR concentrations dramatically increases the rate of pro-σ^E cleavage (Fig. S4*B*). We therefore expected that the modest increase in Spo0A~P activity around the KinA threshold could result in a switch-like ultrasensitive increase in σ^E activity (Fig. S4*B*).

In a combined model of the phosphorelay, σ^F and σ^E modules showed that σ^E activation does increase ultrasensitively as a function of KinA levels induced by different concentrations of IPTG between 4 μM and 10 μM (Fig. 4*A*). The Hill equation fit to σ^E activity as a function of IPTG shows a half-maximal threshold of 7.4 μM IPTG (with a 95% confidence interval of 7.28–7.63 μM) and a Hill coefficient of $n \sim 5$. Around this threshold (from 4 to 10 μM IPTG), we observed only a modest increase in *PspoIIG* transcriptional activity and σ^F activity (see sections above: mean *PspoIIG* transcriptional activity increases ~fivefold, whereas mean σ^F activity increases ~twofold). However, the combined increase in *spoIIG* and *spoIIR* expression was synergistically amplified by the feed-forward loop, resulting in an ~30-fold increase of active σ^E. As a result of this ultrasensitive increase in σ^E activity at the single-cell level, the distribution of σ^E in the population became bimodal (Fig. 4*B*). This allows us to define a threshold of active σ^E concentration (1 μM active σ^E; Fig. 4*B*, dashed line) and robustly predict the fraction of cells that activate σ^E, and thereby commit to sporulation. The fraction

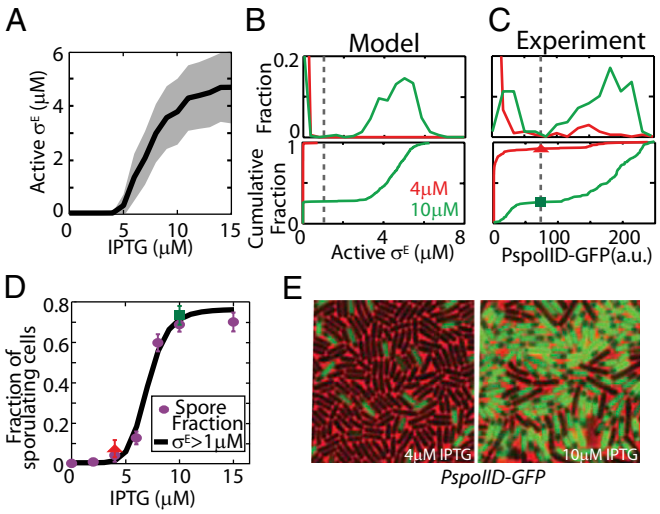

Fig. 4. σ^E activation is the ultrasensitive switch that controls cell fate. (*A*) Stochastic simulations show that σ^E activation (mean response, solid black line; SD, shaded area) increases ultrasensitively in single cells as a function of IPTG and that this threshold coincides with the KinA threshold for sporulation. The mean active σ^E level increases ~30-fold between 4 μM and 10 μM IPTG. Bimodal distributions of active σ^E in the model (*B*, *Upper*) and single-cell experiments (*C*, *Upper*) are shown. In *C*, *PspoIID-gfp* was used as a reporter to track the active σ^E level in single-cell experiments; fluorescence is shown in arbitrary units (a.u.). (*B* and *C*) Cumulative distributions (*Lower*) correspond to the data (*Upper*). Threshold values separating two peaks (vertical gray bars) are chosen to predict the fraction of cells that activate σ^E in *D*. (*D*) Model predictions for the fraction of sporulating cells based on the threshold of the active σ^E level (black curve) are computed using the distributions for various IPTG levels and the threshold value shown in *B*. Experimental data (red triangle and green square for 4 μM and 10 μM, respectively) are obtained using the threshold and distributions in *C*. Both experimental and computationally computed fractions of σ^E-active cells are in excellent agreement with the observed experimental spore fraction (purple dots; calculated from sporulation efficiency, same data as in Fig. 2*C*). (*E*) Examples of microscopy data of strain MF1957 used to construct distributions in *C*. Only a small fraction of cells show σ^E activity (green mother cell in the image) at low IPTG concentrations (*Left*, 4 μM). This fraction increases ultrasensitively at high IPTG (*Right*, 10 μM). The images show a field of view of 30 × 30 μm.

of cells committed to sporulation, as predicted by a threshold concentration of 1 μM active σ^E by T3, increased ultrasensitively between 4 μM and 10 μM IPTG, in good agreement with the change in sporulation faction [Fig. 4*D*; compare the model prediction (black curve) with the fraction of sporulated cells (purple dots; same as in Fig. 3*D*)].

To test our modeling predictions of a bimodal distribution of σ^E activity, we used single-cell measurements of σ^E activity at T3 utilizing *PspoIID-gfp* (MF1957) as a reporter using fluorescence microscopy (Fig. 4 *C*–*E*). These experiments showed that the fraction of cells with active σ^E changes drastically between 4 μM and 10 μM IPTG (Fig. 4*D*). The σ^E-active cells increase from 1.075 ± 0.26% (average ± SD of four measurements; details are provided in *Materials and Methods*) of cells counted at 4 μM to 75.5 ± 3% of cells counted at 10 μM. This dramatic increase agrees well with our model as well as with the measurements of spore fraction in experiments (Fig. 4*D*). As shown in Fig. 4*D*, the red triangle (4 μM) and the green square (10 μM) show the fraction of cells with σ^E activity above the threshold from Fig. 4*C* and match the model predictions (black curve) and the measured fraction of sporulated cells (purple dots). These results show that activation of σ^E can be used as an accurate predictor of cell fate during IPTG-induced sporulation.

The difference in ultrasensitive activation thresholds for σ^F and σ^E (compare Figs. 3D and 4D) suggests that in the 2-μM to 5-μM IPTG range, σ^E activation and, consequently, sporulation are limited primarily by the inadequate expression of *spoIIG*. To test this hypothesis, we first modified our model so that *spoIIG* was expressed constitutively at a level comparable to that seen at 10 μM IPTG (details are provided in *SI Materials and Methods*). Repeating the simulations described above, we found that the fraction of cells that activate σ^E at 4 μM IPTG increases substantially to ~40% in this case (Fig. S5*A*, solid curve). These results suggest that high-level expression of *spoIIG* reduces the IPTG threshold for σ^E activation and the fraction of cells that activate σ^E is determined by the number of cells that activate σ^F (Fig. S5*A*, compare solid and dotted curves). Next, to confirm these predictions experimentally, we constructed a modified ASI strain (MF4883) in which the *spoIIG* operon (including both *spoIIGA* and *spoIIGB*, the gene for pro-σ^E) is expressed constitutively from the *Pspac* promoter (41). In this strain, the LacI operator binding site in the *Pspac* promoter was deleted to allow *spoIIG* to be expressed at high levels during growth independent of the IPTG concentration used to induce *kinA* expression (41). Using the same experimental protocol as above, σ^E activity at T3 for this strain was quantified using a *PspoIID-gfp* reporter. We found that similar to Fig. 5 *B* and *C*, σ^E activity is bimodally distributed in the population at both 4 μM and 10 μM IPTG (Fig. S5 *B* and *C*) even though *spoIIG* is expressed constitutively. However, in contrast to Fig. 5*C*, the fraction of σ^E-active cells in this strain increases only approximately twofold from 37% to 78% between 4 μM and 10 μM IPTG (mean of two independent measurements at each IPTG concentration; Fig. S5 *A* and *C*). These measurements are in excellent agreement with the predictions from our model (Fig. S5*A*). Thus, even at a low level of KinA, the constitutive expression of *spoIIG* increases the fraction of σ^E-active and, consequently, sporulating cells. Taken together, these results reinforce the model that the increase in sporulation at the KinA threshold is mainly due to the ultrasensitive increase in σ^E activation via feed-forward loops involving both transcriptional and posttranslational processes (Fig. 1*A*).

Activation of σ^F Does Not Ensure Successful Sporulation in WT *B. subtilis* Cells. Thus far, from our data based on a combination of mathematical modeling with ASI experiments, we have uncovered two important properties of the sporulation network response: (*i*) Activities of σ^F and σ^E increase ultrasensitively with the increase in Spo0A activation, and (*ii*) at some subthreshold levels of Spo0A activity, cells that activate σ^F may fail to activate σ^E. We therefore ask if these predictions can be tested using WT cells in sporulation-inducing conditions. To this end, we used fluorescence microscopy to measure gene expression in individual WT cells. We note that we have no direct control of the Spo0A activity in this setup, and therefore cannot probe the input–output response of the network directly at the population level. Nevertheless, because Spo0A activity is broadly heterogeneous during starvation (16, 17, 21, 22), correlations between activities of Spo0A and sigma factor can be examined in single cells over a wide range of values. Therefore, to determine if activation of σ^F and σ^E is ultrasensitive to increases in Spo0A activity, we simultaneously measured activities of Spo0A and sigma factors during starvation. We used a triple reporter strain (MF4859) with a σ^F activity reporter (*PspoIIQ-mCherry*) and a σ^E activity reporter (*PspoIID-yfp*), in addition to the Spo0A activity reporter *PspoIIA-cfp*. To ensure that the measured activities are not hindered by differences in local microenvironments or by heterogeneity in sporulation initiation times, we chose to study the effects in liquid sporulation media and thereafter to measure activities of the reporters at several time points following the sporulation. Our results indicate that activity of Spo0A first increased up to T2.5 (for WT cells, T*n* refers to *n* hours after cells were placed in the sporulation media) and then started to decrease, as observed in general (27, 42). This decrease might be associated with the transcriptional repression that occurs at later times, when there is enough active σ^E for the downstream sporulation events.

We therefore focused on the analysis of the reporter activities at T2.5, the time at which many cells have already formed an asymmetrical septum. In agreement with our predictions from the ASI system, starving WT cells showed distinctly bimodal patterns of σ^F and σ^E activity (Fig. S6 *A* and *B*). Such distributions allowed us to choose a threshold for σ^F and σ^E activity separating two peaks

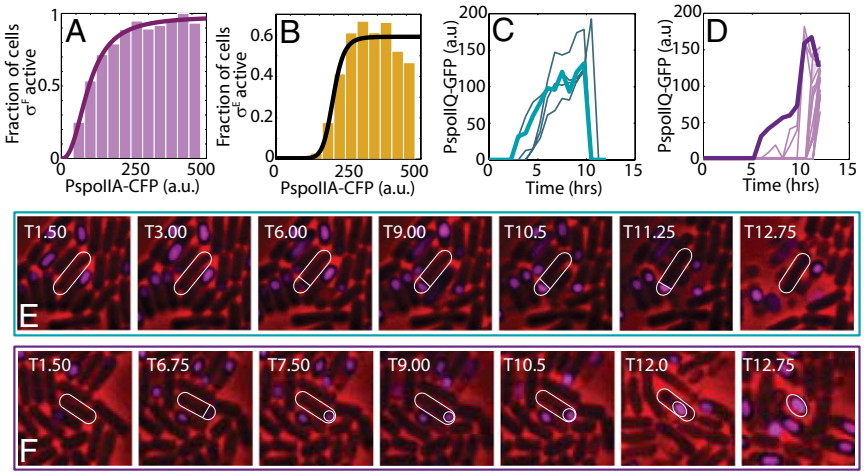

Fig. 5. Ultrasensitivity and cell fate decision in WT cells. (*A* and *B*) Triple reporter strain (MF4859) was used to measure Spo0A and sigma factors activities simultaneously in WT cells grown in starvation media. Cells were binned based on CFP fluorescence for Spo0A activity (*PspoIIA-cfp*), and the fractions of cells in each bin that are σ^F-active and σ^E-active (based on appropriate *PspoIIQ-mCherry* and *PspoIID-yfp* fluorescence thresholds) are shown in *A* and *B*, respectively. The solid lines represent Hill equation fits. These fits indicate that fractions of cells displaying both σ^F and σ^E activities increase ultrasensitively at different Spo0A activity thresholds. (*C* and *D*) Time-lapse microscopy was used to track σ^F activities and cell fates in WT cells (MF1027) under starvation conditions. (*C*) Time-lapse trajectories of σ^F activity in cells that activate σ^F but fail to engulf the forespore and resume growth. (*D*) Time-lapse trajectories of σ^F activity in cells that activate σ^F, engulf the forespore, and form a phase-bright spore. Representative examples of cells that activate σ^F and fail to engulf (*E*) or successfully engulf and form a spore (*F*). σ^F activity (*PspoIIQ-gfp*) is false-colored magenta. Trajectories of σ^F activity for the specific cells shown in *E* and *F* are indicated by thick lines in *C* and *D*, respectively. All fluorescence intensities are reported in arbitrary units (a.u.). The images show a field of view of (E) 8 × 8 μm and (F) 10 × 10 μm.

in bimodal distributions (Fig. S6 *A* and *B*, horizontal dashed gray line), and thereby to classify cells as either σ^F/σ^E-active or -inactive. Strikingly, the number of σ^F/σ^E-active cells depended on the ultrasensitivity of Spo0A activity (Fig. 5 *A* and *B* and Fig. S6 *A* and *B*). In other words, we could define a clear threshold value (Fig. S6 *A* and *B*, vertical dashed gray line) for Spo0A activity required for the activation of the downstream sigma factor. To quantify the ultrasensitivity of σ^F and σ^E activities in response to Spo0A activity, cells were binned according to their activity levels of Spo0A and the fraction of σ^F/σ^E-active cells in each bin was calculated. This analysis yields the fraction of cells with active σ^F/σ^E as a function of Spo0A activity (Fig. 5 *A* and *B*). Using Hill equation fits, we found that the fraction of σ^F-active cells increases ultrasensitively (Hill exponent $n \sim 4$) around a Spo0A activity threshold of ~147 (in arbitrary units of *PspoIIA-cfp* fluorescence; 95% confidence interval: 120–174). Using the same fitting procedure, the fraction of σ^E-active cells was found to increase with even greater sensitivity (Hill exponent $n \sim 10.67$) around a Spo0A activity threshold of ~198 (95% confidence interval: 178–218.5). Notably, the threshold of Spo0A activity and effective Hill coefficient for σ^E activation exceed their corresponding values for σ^F activation. Thus, based on these results, we can conclude that σ^F and σ^E activity increases ultrasensitively as a function Spo0A activity, with σ^E activation occurring more ultrasensitively and at a higher threshold.

Going further, we tried to determine if starving WT cells can indeed fail to sporulate despite activation of σ^F. This question required our ability to track cell fate in a long time sequence of observations, and we therefore used time-lapse microscopy of cells growing in starvation conditions on a solid agarose medium. We note that although we attempted to use a strain expressing two fluorescence reporters (YFP and CFP) for σ^F and σ^E activities, one of the intensities was unstable on the agarose medium (but stable in liquid culture) for unknown reasons. Thus, we decided to use the single-color GFP reporter system for each time-lapse microscopy experiment. With this setup, we first tracked σ^F activity simultaneously with sporulation cell fate. Notably, we found that during starvation, a fraction of WT cells (MF1027) form an asymmetrical septum and activate σ^F but never engulf the forespore (Fig. 5 *C* and *E* and Fig S6*C*). In this fraction, σ^F activity subsequently subsides and cells either become dormant or resume vegetative growth (Fig. 5 *C* and *E*). Because engulfment of the forespore depends entirely on activation of σ^E (43), these results indicate that some fractions of the WT population fail to activate σ^E despite activating σ^F and, as a result, are unable to complete sporulation. It should be noted that failure to activate σ^E in these cells is not manifested by insufficient σ^F activity. Peak σ^F activity in these cells is comparable to that in cells that do engulf the forespore and complete sporulation (compare Fig. 5 *C* and *E* with *D* and *F*). Therefore, failure to activate σ^E must be attributed to other factors. Our results with the ASI system (Figs. 3 and 4) and the results of Fig. 5*B* suggest that insufficient Spo0A activity may be responsible for failure to activate σ^E. Thus, these results verify our prediction that σ^F activation is not always an accurate predictor of cell fate because its activation can be reversed in some circumstances.

By repeating the time-lapse measurements with the strain containing σ^E activity reporter (MF248), we found that expression patterns of the reporter gene are quite distinct from those for σ^F activity reporter (Fig. S6 *D* and *E*). We find that the majority, if not all, of the cells that activate σ^E successfully engulf the forespore and proceed to sporulation. Although some cells that activate σ^E died before completion of sporulation, few or no σ^E-active cells were observed to resume vegetative growth. These results are consistent with previous reports indicating that σ^E activation is the sporulation commitment point (23, 24, 37). Notably, in these reports, it was also suggested that all WT cells that form an asymmetrical septum eventually activate σ^F and σ^E and reach the commitment point unless the environment is changed (e.g., by resuspension in nutrient-rich media). In contrast, our results indicate that even under unchanging starvation conditions, a fraction of cells activate σ^F but never reach the point of σ^E activation.

Taken together, our results with WT cells in sporulation conditions confirm the predictions made based on the ASI system and mathematical modeling. We suggest that different thresholds for σ^F and σ^E activation may allow cells to reverse their developmental progression, even after activating σ^F, and thereby protect them from unnecessary time and energy.

Discussion

Gene regulatory networks controlling cellular differentiation can be viewed as analog-to-digital converters, because their functions are to sense various signals from the environment and to process these signals to induce the transition of cell types to one of discrete states (44). This conversion of the environmental signals into a cell fate decision can be described phenomenologically by simply postulating an activity threshold of the master regulatory component of the differentiation network. In prokaryotes, several master transcription factors that determine cell fate in response to environmental conditions have been reported, including CtrA for the *Caulobacter crescentus* cell cycle (45), ComK fo *B. subtilis* competence development (46), and Spo0A for *B. subtilis* sporulation (10).

However, due to the limitation of methods used, previous studies do not provide a mechanistic understanding of how these thresholds originate or how variable they are in the population. Here, our goal was to understand how signals are processed and how the cell fate decisions are made in sporulating *B. subtilis* cells. In this organism under starvation conditions, multiple environmental signals, some yet unknown, converge on the phosphorelay network, resulting in noisy, highly variable activation of the Spo0A master regulator. We therefore needed to uncover how the heterogeneous increases in Spo0A activity affect the cell decision to sporulate. In other words, we seek the cell decision point in the sporulation network at which the noisy, continuous, but heterogeneous distributions of Spo0A activity are transformed into discrete subpopulations associated with specific cell fates. Taking advantage of a synthetic strain, in which the levels of Spo0A activity can be externally controlled by the inducer IPTG (27) and multireporter strains in WT background, we found that:

i) Despite the presence of positive transcriptional feedbacks in the phosphorelay module, an increase in the inducer leads to a graded (nonultrasensitive) increase in the Spo0A~P concentration. The graded nature of this response leads to unimodal distributions of expressions of Spo0A~P targets with no clear threshold that can be used to define cell fate robustly. Thus, the ultimate decision for sporulation occurs downstream of the phosphorelay module.

ii) An increase in Spo0A~P concentration leads to a switch-like increase in σ^F activity in the forespore. However, the fraction of cells that activate σ^F under certain conditions can significantly exceed the fraction of cells that sporulate. Therefore, activation of σ^F does not ensure completion of sporulation, and it is not an accurate predictor of cell fate.

iii) The synergistic interaction between the phosphorelay (Spo0A activation) module and the σ^F module results in an ultrasensitive increase in σ^E activity in the mother cell. This ultrasensitivity produces a bimodal ON-or-OFF distribution of σ^E activity in the population. As a result, most of cells with active σ^E produce spores, indicating that the stage of σ^E activation is the ultimate sporulation decision point.

iv) WT *B. subtilis* cells under starvation conditions show an ultrasensitive relation between the activity of Spo0A and activation of σ^F and σ^E in single cells. Cells that activate σ^E complete sporulation, whereas cells that activate σ^F can sometimes

fail to engulf the forespore and, instead, resume growth or become dormant.

Examination of these results in light of the architecture of the sporulation network (Fig. 1 *A* and *B*) suggests that the design of the ultrasensitive switch that determines cell fate in sporulation is quite unique. In many other organisms, the cell fate decision has been shown to be controlled by the ultrasensitive activation of the master regulator through positive feedback, resulting in a bistable response. Thus, two stable states of the responses correspond to two distinct cell fates (47–53). Surprisingly, despite the presence of positive feedback in the phosphorelay architecture, we have found that the phosphorelay response to KinA induction is graded and nonultrasensitive. This is a unique and crucial design feature, with which the sporulation network avoids the slowdown in the dynamical response that is characteristic of bistable systems (51, 54, 55). Instead, the sporulation network generates an ultrasensitive response by using a cascade of coherent feed-forward loops combining transcriptional and posttranslational interactions. Specifically, Spo0A∼P, in a concentration-dependent manner, directly controls the expression of both σ^F and σ^E and indirectly controls their activation. The mother cell-specific activation of σ^E is therefore under the control of a cascade of two intercompartmental coherent AND-type feed-forward loops (Fig. 1*C*). Around the KinA threshold, all the branches of each of the cascades are activated, leading to a highly ultrasensitive increase in the level of active σ^E. Perturbations of this architecture decrease the threshold and sensitivity of the sporulation response (Fig. S5).

Surprisingly, our results show that although most cells fail to activate sufficient levels of σ^E at subthreshold KinA levels, many cells express sufficient levels of Spo0A∼P to form an asymmetrical septum and even to activate σ^F. From a design perspective, this response at subthreshold levels of KinA appears somewhat wasteful and unnecessary. However, in contrast to the well-controlled conditions of the ASI system, under unpredictable starvation conditions, WT cells need to make cell fate decisions based on noisy information that is encoded into a widely fluctuating Spo0A∼P level. To make a timely and accurate decision under such conditions, the cell has to collect information about the environment for a certain period to average out the noisy fluctuations of signals and noise of its own biochemical processes. By deferring the decision to a stage downstream of Spo0A∼P, the cell gains a time-averaging interval for filtering out noisy fluctuations while retaining responsiveness to environmental signals at the Spo0A∼P and phosphorelay levels. It is not surprising then that the sporulation network decision is, in fact, deferred to the stage of σ^E activation. By deferring the decision to this point of sporulation commitment, cells maximize the time-averaging interval that they can use to filter out noisy signals.

Despite our initial focus on the sporulation decision in the ASI system, we had several reasons to expect that these results apply even to WT cells. In particular, we have previously shown that ASI cells under nutrient-rich conditions expressing KinA levels similar to those in the starving WT cells lead to efficient sporulation, similar to the starving WT cells (21, 27). Furthermore, our results (Fig. 2*D*) regarding the unimodality of the expression of Spo0A∼P target genes are in agreement with those of previous reports that studied the phosphorelay response of WT cells in starvation conditions (16, 17, 21). Taking all these results into consideration, we expect that the ASI system can effectively mimic the natural sporulation network despite differences in KinA regulation and a lack of other environmental inputs.

In accordance with these expectations, the results of our experiments with the WT strain in sporulation conditions are consistent with the major predictions made using the ASI system. σ^F and σ^E activation in single WT *B. subtilis* cells under starvation conditions does indeed increase ultrasensitivity at a threshold level of Spo0A activity. Although our measurements indicate that σ^E is activated at a higher threshold, it is difficult to determine these thresholds accurately in the WT setting due to the large heterogeneity of Spo0A activity. This illustrates the utility of the ASI system, because it offers a mode of control over Spo0A activation. Nevertheless, using time-lapse microscopy, we were able to verify the occurrence of cells that activate σ^F and yet fail to complete sporulation successfully. Because these cells never engulf the forespore, we concluded that the failure to complete sporulation results from a lack of σ^E activity. On the other hand, most of the cells that activate σ^E were found to complete engulfment and proceed to sporulation. Therefore, even in the WT setting, σ^F activation alone overestimates the sporulation response of the population, albeit far less strikingly than in the ASI system at a low KinA. Given these ultrasensitive cell fate-determining relationships between activities of Spo0A and σ^F and σ^E, we believe more detailed comparisons between the ASI and WT dynamics in future studies may allow us to uncover how specific environmental signals influence sporulation.

Materials and Methods

Modeling Methods. To uncover how the increase in KinA expression affects sporulation, we built a detailed mathematical model of the sporulation network based on its known topology. For this, the network was divided into three modules that play essential roles in the early phases of sporulation in a hierarchical order: (*i*) the phosphorelay that controls Spo0A activation, (*ii*) the σ^F activation module in the forespore compartment, and (*iii*) the σ^E activation module in the mother cell compartment (Fig. 1*C*). We briefly discuss the model here and refer the reader to *SI Materials and Methods* and Table S3 for details.

To study the function of each module, we modeled its input–output functions separately. The input and output signals for the phosphorelay module can be defined as the level of KinA and the resulting Spo0A∼P level, respectively (Fig. 1*B*). In turn, Spo0A∼P, as the input, governs the forespore-specific activation of σ^F by controlling the transcription of the *spoIIA* operon (encoding σ^F and its two regulators) and the *spoIIE* gene (8) (encoding the serine phosphatase required for the activation of σ^F; Fig. 1*C*). Immediately after forespore formation, Spo0A∼P in the mother cell and active σ^F in the forespore act as inputs for the σ^E module, and thus control expression of the σ^E regulon as the output (8, 38). Details of all posttranslational interactions and transcriptional regulation, as well as relevant parameter values (Table S3), were extracted from the literature (5, 8, 12, 16, 32, 33, 36, 40, 55–57).

We studied both the steady-state and dynamical properties of each module. First, we used the ode45 simulator of MATLAB (MathWorks) to study the deterministic response of each network module. Global parameter sampling for the phosphorelay was used to determine if steady-state Spo0A∼P concentrations can increase ultrasensitively between 4 μM and 10 μM IPTG. Subsequently, stochastic simulations for different IPTG doses were performed using the SSA algorithm of the StochKit package (58). An ensemble of 400 trajectories of the phosphorelay response to each IPTG concentration was used to estimate average response times (Fig. S2) and distributions of *spoIIA*, *spoIIE*, and *spoIIG* gene expression levels.

Variability in the expression of these genes combined with the ultrasensitive activation of σ^F and σ^E produces bimodal distributions of sigma factor activities (Figs. 3*B* and 4*B* and Figs. S3 and S4). A threshold level of σ^F can be used to divide the population into σ^F-active and σ^F-inactive fractions. We chose a threshold of 2 μM σ^F, which lies between the two modes of the σ^F distribution, to ensure that the predicted fractions of σ^F-active cells are least sensitive to variations in this threshold. To predict cell fate based on σ^F, all cells above this threshold are counted as sporulating cells (Fig. 3*D*, black line). Similarly, we define 1 μM σ^E (between the modes of σ^E distributions) as a threshold to predict fractions of active cells robustly. To predict cell fate based on these distributions, all cells above the threshold of 1 μM σ^E were counted as sporulating cells (Fig. 4*D*, black line). The fraction of sporulating cells predicted based on σ^F and σ^E activities was subsequently compared with the fraction of sporulating cells calculated from measurements of sporulation efficiencies as described in the next section.

Estimation of Fraction of Sporulating Cells from Spore Counts. Heat shock-resistant spore counts and total viable cell counts (spores + vegetative cells) at each IPTG dose were estimated as described in *Experimental Materials and Methods*. Spore counts were measured at least three times at each IPTG concentration indicated in Fig. 1*D*. To calculate the fraction of sporulating cells (Figs. 3*D* and 4*D*), we first compute sporulation efficiency (i.e., the ratio of spores to viable cells that is observed at the end of the experiment). To

calculate the efficiency, each spore count was normalized by the total viable cell counts measured at the respective IPTG concentrations. We note that total viable cell count varies only ~10% between 0 μM and 20 μM IPTG, whereas spore counts change more than 20-fold. As a result, there is relatively little effect of total cell count variability on sporulation efficiency and the KinA threshold effect is reproducible. We therefore normalize the three independent measurements of spore counts at each IPTG concentration by the average total viable cell count to determine three measurements of sporulation fraction at each IPTG dose. These calculated sporulation efficiencies can subsequently be used to determine the fraction of sporulating cells reliably.

The fraction of sporulating cells (f) is underrepresented in the final viable cell counts because nonsporulating cells can further divide and increase their numbers, whereas spores do not divide. To account for this in our estimate of the fraction f, we establish a relation between the sporulation (p) and the actual fraction of cells that chose to sporulate (f). Assuming that the population size was N before nutrients became too scarce for sporulation, the number of spores in the final population is Nf and the number of nonspores is $2^n N(1-f)$ because the nonspores divide n times. Accordingly, the sporulation efficiency (p) is related to the fraction of sporulating cells (f) as:

$$p = \frac{Nf}{Nf + 2^n N(1-f)} = \frac{f}{f + 2^n(1-f)} \Rightarrow f = \frac{2^n p}{1 + (2^n - 1)p}, \quad [1]$$

where n is the average number of times that a cell that does not sporulate will divide. Based on experimental observations, we find that $n \sim 2$. We use this relationship to calculate the fraction of sporulating cells and compare f with the fraction predicted by our simulations (Figs. 3*D* and 4*D*).

Experimental Materials and Methods

Strain Construction. The parental strain for all experiments was *B. subtilis* PY79. Strains used and generated in this study are listed in Table S1. Detailed information about the ASI system (*Phy-spank-kinA*) can be found elsewhere (21, 28). CFP, YFP, and mCherry reporter genes were amplified by PCR using the primers listed in Table S2. DNAs of pDR201 harboring the gene for mCherry, *B. subtilis* strain BTD217 (*amyE::PspoIIQ-RBSopt-cfp-spoIIQ*) and *B. subtilis* strain BKM1563 (*ycgO::PspoIVF-spoIVFB-yfp*) (both gifts from David Rudner, Harvard Medical School, Boston, MA) were used as templates for PCR. Promoter DNA fragments for *spoIIQ* and *spoIID* were amplified from *B. subtilis* PY79 strain using the primers listed in Table S2. After restriction enzyme digestion (as listed in Table S2), each of the DNA fragments was cloned into either pDG1730 (*amyE* integration vector) (59) or pDG1664 (*thrC* integration vector) (59). Plasmids generated were inserted by double-crossover recombination into either the *amyE* or *thrC* locus of the chromosome of *B. subtilis* PY79 strain. *PspoIIA-cfp* (a gift from Jan-Willem Veening, University of Groningen, Groningen, The Netherlands) was constructed as described (60). GFP reporter strains were published previously (38). Details of the constructions are available on request.

Media and Sporulation Conditions. Sporulation of the ASI strain was induced in LB by adding IPTG at the indicated concentrations as described previously (21). Sporulation in the WT strain background was induced by the procedure of Sterlini and Mandelstam (61).

Sporulation and β-Galactosidase Assays. Assays for sporulation and β-galactosidase activity were performed as described previously (21).

Fluorescence and Time-Lapse Microscopy. Fluorescence microscopy was performed as described previously (62). In brief, cells from 0.2 mL of culture were centrifuged and suspended in 50 μL of 1 × PBS. The concentrated cell suspension (2 μL) was placed on 1% (wt/vol) agarose pads containing 1 × PBS within a 25-μL Gene Frame (AB Gene) covered by a clean microscope slide coverslip and was viewed using an Olympus BL51 fluorescence microscope with Slidebook software (Intelligent Imaging Innovations). For Figs. 3*C* and 4*C*, fluorescence measurements of σ^F and σ^E activities at 4 μM and 10 μM IPTG were made for multiple colonies (five colonies for σ^F and four colonies for σ^E; each colony had ~100 cells). These fluorescence measurements were used, along with appropriate thresholds, to count the number of cells that are sigma-active in each colony. The mean and SD of the fractions are reported as percentages. Histograms of sigma factor activities in individual colonies are provided in Figs. S3*F* and S4*E*.

Time-lapse microscopy was performed by the procedure of de Jong et al. (63) using the fluorescence microscope with a temperature-controlled chamber from Solent Scientific. In brief, sporulating cells incubated for 1 h at 37 °C in the medium of Sterlini and Mandelstam (61) were spotted on 1% (wt/vol) agarose pads containing the identical medium within a 25-μL Gene Frame and covered by a clean microscope slide coverslip. A prepared slide glass was placed in the prewarmed (37 °C) environmental chamber of the microscope and monitored single cells over time. Intensities of fluorescent proteins (arbitrary units per pixel) in cells were analyzed electronically with Slidebook software and customized MATLAB code.

ACKNOWLEDGMENTS. We thank David Rudner and Jan-Willem Veening for the YFP, CFP, and mCherry strains. We also thank Hoang-Anh Dao for technical assistance. This study was financially supported by National Science Foundation Grant MCB-0920463 (primary investigator, M.F.; coprimary investigator, O.A.I.) and a Howard Hughes Medical Institute International Student Research Fellowship (to J.N.). The simulations were performed using a system supported by the National Science Foundation under Grants CNS-0821727 and OCI-0959097.

1. Errington J (2003) Regulation of endospore formation in Bacillus subtilis. *Nat Rev Microbiol* 1(2):117–126.
2. Nicholson WL, Munakata N, Horneck G, Melosh HJ, Setlow P (2000) Resistance of Bacillus endospores to extreme terrestrial and extraterrestrial environments. *Microbiol Mol Biol Rev* 64(3):548–572.
3. Errington J (1993) Bacillus subtilis sporulation: Regulation of gene expression and control of morphogenesis. *Microbiol Rev* 57(1):1–33.
4. Fawcett P, Eichenberger P, Losick R, Youngman P (2000) The transcriptional profile of early to middle sporulation in Bacillus subtilis. *Proc Natl Acad Sci USA* 97(14): 8063–8068.
5. Eichenberger P, et al. (2003) The sigmaE regulon and the identification of additional sporulation genes in Bacillus subtilis. *J Mol Biol* 327(5):945–972.
6. Wang ST, et al. (2006) The forespore line of gene expression in Bacillus subtilis. *J Mol Biol* 358(1):16–37.
7. Piggot PJ, Coote JG (1976) Genetic aspects of bacterial endospore formation. *Bacteriol Rev* 40(4):908–962.
8. Hilbert DW, Piggot PJ (2004) Compartmentalization of gene expression during Bacillus subtilis spore formation. *Microbiol Mol Biol Rev* 68(2):234–262.
9. Molle V, et al. (2003) The Spo0A regulon of Bacillus subtilis. *Mol Microbiol* 50(5): 1683–1701.
10. Hoch JA (1993) The phosphorelay signal transduction pathway in the initiation of Bacillus subtilis sporulation. *J Cell Biochem* 51(1):55–61.
11. Hoch JA (1993) Regulation of the phosphorelay and the initiation of sporulation in Bacillus subtilis. *Annu Rev Microbiol* 47:441–465.
12. Burbulys D, Trach KA, Hoch JA (1991) Initiation of sporulation in B. subtilis is controlled by a multicomponent phosphorelay. *Cell* 64(3):545–552.
13. Veening JW, Smits WK, Kuipers OP (2008) Bistability, epigenetics, and bet-hedging in bacteria. *Annu Rev Microbiol* 62:193–210.
14. Schultz D, Wolynes PG, Ben Jacob E, Onuchic JN (2009) Deciding fate in adverse times: Sporulation and competence in Bacillus subtilis. *Proc Natl Acad Sci USA* 106(50): 21027–21034.
15. Bischofs IB, Hug JA, Liu AW, Wolf DM, Arkin AP (2009) Complexity in bacterial cell-cell communication: Quorum signal integration and subpopulation signaling in the *Bacillus subtilis* phosphorelay. *Proc Natl Acad Sci USA* 106(16):6459–6464.
16. Chastanet A, et al. (2010) Broadly heterogeneous activation of the master regulator for sporulation in *Bacillus subtilis*. *Proc Natl Acad Sci USA* 107(18):8486–8491.
17. de Jong IG, Veening JW, Kuipers OP (2010) Heterochronic phosphorelay gene expression as a source of heterogeneity in Bacillus subtilis spore formation. *J Bacteriol* 192(8):2053–2067.
18. Morohashi M, et al. (2007) Model-based definition of population heterogeneity and its effects on metabolism in sporulating Bacillus subtilis. *J Biochem* 142(2):183–191.
19. Ben-Yehuda S, Losick R (2002) Asymmetric cell division in B. subtilis involves a spiral-like intermediate of the cytokinetic protein FtsZ. *Cell* 109(2):257–266.
20. Levin PA, Losick R (1996) Transcription factor Spo0A switches the localization of the cell division protein FtsZ from a medial to a bipolar pattern in Bacillus subtilis. *Genes Dev* 10(4):478–488.
21. Eswaramoorthy P, Dinh J, Duan D, Igoshin OA, Fujita M (2010) Single-cell measurement of the levels and distributions of the phosphorelay components in a population of sporulating Bacillus subtilis cells. *Microbiology* 156(Pt 8):2294–2304.
22. Levine JH, Fontes ME, Dworkin J, Elowitz MB (2012) Pulsed feedback defers cellular differentiation. *PLoS Biol* 10(1):e1001252.
23. Dworkin J, Losick R (2005) Developmental commitment in a bacterium. *Cell* 121(3): 401–409.
24. Kuchina A, Espinar L, Garcia-Ojalvo J, Süel GM (2011) Reversible and noisy progression towards a commitment point enables adaptable and reliable cellular decision-making. *PLOS Comput Biol* 7(11):e1002273.
25. Xenopoulos P, Piggot PJ (2011) Regulation of growth of the mother cell and chromosome replication during sporulation of Bacillus subtilis. *J Bacteriol* 193 (12):3117–3126.
26. Bashor CJ, Horwitz AA, Peisajovich SG, Lim WA (2010) Rewiring cells: Synthetic biology as a tool to interrogate the organizational principles of living systems. *Annu Rev Biophys* 39:515–537.

27. Eswaramoorthy P, et al. (2010) The threshold level of the sensor histidine kinase KinA governs entry into sporulation in Bacillus subtilis. *J Bacteriol* 192(15):3870–3882.
28. Fujita M, Losick R (2005) Evidence that entry into sporulation in Bacillus subtilis is governed by a gradual increase in the level and activity of the master regulator Spo0A. *Genes Dev* 19(18):2236–2244.
29. Seredick SD, Seredick BM, Baker D, Spiegelman GB (2009) An A257V mutation in the bacillus subtilis response regulator Spo0A prevents regulated expression of promoters with low-consensus binding sites. *J Bacteriol* 191(17):5489–5498.
30. Schmidt R, et al. (1990) Control of developmental transcription factor sigma F by sporulation regulatory proteins SpoIIAA and SpoIIAB in Bacillus subtilis. *Proc Natl Acad Sci USA* 87(23):9221–9225.
31. Errington J, et al. (1996) Control of the cell-specificity of sigma F activity in Bacillus subtilis. *Philos Trans R Soc Lond B Biol Sci* 351(1339):537–542.
32. Clarkson J, Campbell ID, Yudkin MD (2004) Efficient regulation of sigmaF, the first sporulation-specific sigma factor in B. subtilis. *J Mol Biol* 342(4):1187–1195.
33. Iber D, Clarkson J, Yudkin MD, Campbell ID (2006) The mechanism of cell differentiation in Bacillus subtilis. *Nature* 441(7091):371–374.
34. Igoshin OA, Price CW, Savageau MA (2006) Signalling network with a bistable hysteretic switch controls developmental activation of the sigma transcription factor in Bacillus subtilis. *Mol Microbiol* 61(1):165–184.
35. Mangan S, Alon U (2003) Structure and function of the feed-forward loop network motif. *Proc Natl Acad Sci USA* 100(21):11980–11985.
36. Lewis RJ, et al. (2002) Dimer formation and transcription activation in the sporulation response regulator Spo0A. *J Mol Biol* 316(2):235–245.
37. Fujita M, González-Pastor JE, Losick R (2005) High- and low-threshold genes in the Spo0A regulon of Bacillus subtilis. *J Bacteriol* 187(4):1357–1368.
38. Eldar A, et al. (2009) Partial penetrance facilitates developmental evolution in bacteria. *Nature* 460(7254):510–514.
39. Fujita M, Losick R (2003) The master regulator for entry into sporulation in Bacillus subtilis becomes a cell-specific transcription factor after asymmetric division. *Genes Dev* 17(9):1166–1174.
40. Hofmeister AE, Londoño-Vallejo A, Harry E, Stragier P, Losick R (1995) Extracellular signal protein triggering the proteolytic activation of a developmental transcription factor in B. subtilis. *Cell* 83(2):219–226.
41. Fujita M, Losick R (2002) An investigation into the compartmentalization of the sporulation transcription factor sigmaE in Bacillus subtilis. *Mol Microbiol* 43(1):27–38.
42. Eichenberger P, Fawcett P, Losick R (2001) A three-protein inhibitor of polar septation during sporulation in Bacillus subtilis. *Mol Microbiol* 42(5):1147–1162.
43. Balázsi G, van Oudenaarden A, Collins JJ (2011) Cellular decision making and biological noise: from microbes to mammals. *Cell* 144(6):910–925.
44. Quon KC, Marczynski GT, Shapiro L (1996) Cell cycle control by an essential bacterial two-component signal transduction protein. *Cell* 84(1):83–93.
45. van Sinderen D, et al. (1995) comK encodes the competence transcription factor, the key regulatory protein for competence development in Bacillus subtilis. *Mol Microbiol* 15(3):455–462.
46. Doncic A, Falleur-Fettig M, Skotheim JM (2011) Distinct interactions select and maintain a specific cell fate. *Mol Cell* 43(4):528–539.
47. Dubnau D, Losick R (2006) Bistability in bacteria. *Mol Microbiol* 61(3):564–572.
48. Malleshaiah MK, Shahrezaei V, Swain PS, Michnick SW (2010) The scaffold protein Ste5 directly controls a switch-like mating decision in yeast. *Nature* 465(7294): 101–105.
49. Melen GJ, Levy S, Barkai N, Shilo BZ (2005) Threshold responses to morphogen gradients by zero-order ultrasensitivity. *Mol Syst Biol* 1:2005.0028.
50. Narula J, Smith AM, Gottgens B, Igoshin OA (2010) Modeling reveals bistability and low-pass filtering in the network module determining blood stem cell fate. *PLOS Comput Biol* 6(5):e1000771.
51. Smits WK, Kuipers OP, Veening J-W (2006) Phenotypic variation in bacteria: The role of feedback regulation. *Nat Rev Microbiol* 4(4):259–271.
52. Tiwari A, Balázsi G, Gennaro ML, Igoshin OA (2010) The interplay of multiple feedback loops with post-translational kinetics results in bistability of mycobacterial stress response. *Phys Biol* 7(3):036005.
53. Tiwari A, Ray JC, Narula J, Igoshin OA (2011) Bistable responses in bacterial genetic networks: Designs and dynamical consequences. *Math Biosci* 231(1):76–89.
54. Sciammas R, et al. (2011) An incoherent regulatory network architecture that orchestrates B cell diversification in response to antigen signaling. *Mol Syst Biol* 7:495.
55. Chastanet A, Losick R (2011) Just-in-time control of Spo0A synthesis in Bacillus subtilis by multiple regulatory mechanisms. *J Bacteriol* 193(22):6366–6374.
56. Fujita M, Sadaie Y (1998) Feedback loops involving Spo0A and AbrB in in vitro transcription of the genes involved in the initiation of sporulation in Bacillus subtilis. *J Biochem* 124(1):98–104.
57. Grimshaw CE, et al. (1998) Synergistic kinetic interactions between components of the phosphorelay controlling sporulation in Bacillus subtilis. *Biochemistry* 37(5):1365–1375.
58. Sanft KR, et al. (2011) StochKit2: Software for discrete stochastic simulation of biochemical systems with events. *Bioinformatics* 27(17):2457–2458.
59. Guérout-Fleury AM, Frandsen N, Stragier P (1996) Plasmids for ectopic integration in Bacillus subtilis. *Gene* 180(1-2):57–61.
60. Veening JW, Smits WK, Hamoen LW, Jongbloed JD, Kuipers OP (2004) Visualization of differential gene expression by improved cyan fluorescent protein and yellow fluorescent protein production in Bacillus subtilis. *Appl Environ Microbiol* 70(11): 6809–6815.
61. Sterlini JM, Mandelstam J (1969) Commitment to sporulation in Bacillus subtilis and its relationship to development of actinomycin resistance. *Biochem J* 113(1):29–37.
62. Eswaramoorthy P, Guo T, Fujita M (2009) In vivo domain-based functional analysis of the major sporulation sensor kinase, KinA, in Bacillus subtilis. *J Bacteriol* 191(17): 5358–5368.
63. de Jong IG, Beilharz K, Kuipers OP, Veening JW (2011) Live Cell Imaging of Bacillus subtilis and Streptococcus pneumoniae using Automated Time-lapse Microscopy. *J Vis Exp* 53:pii: 3145, doi: 10.3791/3145.